Published in final edited form as:
J Neurosci. 2013 May 8; 33(19): 8411–8422. doi:10.1523/JNEUROSCI.3285-12.2013.

In vivo stimulus-induced vasodilation occurs without IP_3 receptor activation and may precede astrocytic calcium increase

Krystal Nizar[1,*], **Hana Uhlirova**[2,*], **Peifang Tian**[3,4], **Payam A. Saisan**[3], **Qun Cheng**[3], **Lidia Reznichenko**[3], **Kimberly L. Weldy**[3], **Tyler C. Steed**[1], **Vishnu B. Sridhar**[5], **Christopher L. MacDonald**[5], **Jianxia Cui**[5], **Sergey L. Gratiy**[2], **Sava Sakadžić**[6], **David A. Boas**[6], **Thomas I. Beka**[3,7], **Gaute T. Einevoll**[7], **Ju Chen**[8], **Eliezer Masliah**[3], **Anders M. Dale**[2,3], **Gabriel A. Silva**[5,9], and **Anna Devor**[2,3,6]

[1]Neurosciences Graduate Program, UCSD, La Jolla, CA 92093

[2]Department of Radiology, UCSD, La Jolla, CA 92093

[3]Department of Neurosciences, UCSD, La Jolla, CA 92093

[4]Department of Physics, John Carroll University, University Heights, OH 44118

[5]Department of Bioengineering, UCSD, La Jolla, CA 92093

[6]Martinos Center for Biomedical Imaging, MGH, Harvard Medical School, Charlestown, MA 02129

[7]CIGENE, Department of Mathematical Sciences and Technology, Norwegian University of Life Sciences, N-1432 As, Norway

[8]Department of Medicine, UCSD, La Jolla, CA 92093

[9]Department of Ophthalmology, UCSD, La Jolla, CA 92093

Abstract

Calcium-dependent release of vasoactive gliotransmitters is widely assumed to trigger vasodilation associated with rapid increases in neuronal activity. Inconsistent with this hypothesis, intact stimulus-induced vasodilation was observed in inositol 1,4,5-triphosphate (IP_3) type-2 receptor (R2) knockout (KO) mice, in which the primary mechanism of astrocytic calcium increase – the release of calcium from intracellular stores following activation of an IP_3-dependent pathway – is lacking. Further, our results in wild type (WT) mice indicate that *in vivo* onset of astrocytic calcium increase in response to sensory stimulus could be considerably delayed relative to the simultaneously measured onset of arteriolar dilation. Delayed calcium increases in WT mice were observed in both astrocytic cell bodies and perivascular endfeet. Thus, astrocytes may not play a role in the initiation of blood flow response, at least not via calcium-dependent mechanisms. Moreover, an increase in astrocytic intracellular calcium was not required for normal vasodilation in the IP_3R_2-KO animals.

Keywords

astrocyte; two-photon microscopy; blood flow; somatosensory cortex; neurovascular coupling

Corresponding author: Anna Devor, 9500 Gilman Drive MC 0624, La Jolla, CA 92093-0624, Tel: (858) 353 3315, Fax: (858) 822 1753, adevor@ucsd.edu.

*These authors contributed equally to this work

The authors declare no conflict of interests

Introduction

A growing body of literature indicates that astrocytes not only provide metabolic support for neurons (Magistretti et al., 1999, Rouach et al., 2008, Halassa et al., 2010, Allaman et al., 2011) but also are capable of calcium-dependent synthesis of vasodilators and vasoconstrictors (vasoactive "gliotransmitters") (Volterra and Meldolesi, 2005). Thus, astrocytes might play a role in the local regulation of microvascular diameters and the resultant blood flow changes accompanying changes in neuronal activity (for recent reviews, see (Iadecola and Nedergaard, 2007, Agulhon et al., 2008, Koehler et al., 2009, Nimmerjahn, 2009, Attwell et al., 2010, Paulson et al., 2010, Petzold and Murthy, 2011)). In brain slices, an increase in astrocytic intracellular calcium causes a slow dilation or constriction of the embedded arteriolar segments (Simard et al., 2003, Zonta et al., 2003, Gordon et al., 2008). A transient increase in astrocytic calcium has also been observed *in vivo* in various parts of the cerebral cortex – somatosensory, visual, and olfactory – in response to the appropriate sensory stimulus or voluntary movement (Wang et al., 2006, Dombeck et al., 2007, Petzold et al., 2008, Schummers et al., 2008, Thrane et al., 2012). However, it remains unclear whether astrocytic calcium increase is required for the initiation of functional hyperemia *in vivo* and whether its onset precedes the onset of vasodilation, as would be expected if the former triggered the latter.

In the present study, we examined the importance of astrocytic calcium signaling for stimulus-induced vasodilation by employing inositol 1,4,5-triphosphate (IP_3) type-2 receptor (R2) knockout (KO) mice lacking the primary mechanism of astrocytic calcium increase (Li et al., 2005, Petravicz et al., 2008). We used *in vivo* two-photon microscopy for parallel imaging of neuroglial calcium dynamics and diameter changes in nearby arterioles in the primary somatosensory cortex (SI) in response to a brief sensory stimulus. IP_3R2-KO mice exhibited no detectable calcium signaling though they did show intact stimulus-induced vasodilation, suggesting that elevation of astrocytic calcium was not required for neurovascular coupling.

We next investigated the temporal relationship between astrocytic increases in intracellular calcium and vasodilation in wild type (WT) mice. Our results demonstrate that the onset of astrocytic calcium transients may be too slow to account for the onset of vasodilation. In addition, while vasodilation and neuronal calcium increase were observed consistently in response to each stimulus trial, the delayed astrocytic calcium increase was only detected in a small percentage of astrocytes, occasionally responding in some of the trials.

The present results do not question the well-established fact that astrocytes house a machinery to synthesize and release substances with vasoactive properties. Rather, they challenge the hypothesis that astrocytes serve as mediators in neurovascular coupling in the healthy brain in response to a brief sensory stimulus – the relevant condition for event-related functional imaging studies.

Materials and Methods

Animal procedures

All experimental procedures were performed in accordance with the guidelines established by the UCSD Institutional Animal Care and Use Committee (IACUC). We used 49 adult mice of either sex: 36 ICR mice and 13 inositol 1,4,5-triphosphate (IP_3) type-2 receptor (R2) knockout (KO) Black Swiss mice. IP_3R2-KO mice were kindly provided by Dr. Ju Chen. Mice were anesthetized with isoflurane during surgical procedures (2% initially, 0.5–1% during all procedures). A cannula was inserted into the femoral artery. A metal holding bar was glued to the temporal bone for immobilization of the head during imaging. An area of

skull overlying the forepaw region of the primary somatosensory cortex (SI) contralateral to the holding bar was exposed and dura mater removed. To avoid herniation of the exposed brain due to excessive intracranial pressure, the dura mater over the IVth cerebral ventricle was punctured, thus allowing drainage of CSF.

Calcium indicator Oregon Green 488 BAPTA-1 AM (OGB1) (O-6807, Invitrogen, 50 μg) was first dissolved in 4 μl of 20% pluronic in DMSO (F-127, Invitrogen); 80 μl of artificial CSF (ACSF) containing 142 mM NaCl, 5 mM KCl, 10 mM glucose, 10 mM Hepes, 3.1 mM $CaCl_2$, 1.3 mM $MgCl_2$, pH 7.4 were added to OGB1 solution to yield a final concentration of 0.5 mM OGB1. OGB1 solution was pressure-microinjected into the cortical tissue (Stosiek et al., 2003) at the location of the maximal neuronal response to forepaw stimulation, mapped prior to imaging using surface potential recordings (Devor et al., 2007). The red fluorescent dye sulforhodamine 101 (SR101, S7635, Sigma) in ACSF was applied topically for ~2 min to label astrocytes (Nimmerjahn et al., 2004). The excess dye was washed with ACSF. A drop of agarose (1% wt/vol, A9793, Sigma) in ACSF was applied on the brain surface, and the exposure was covered with a round glass coverslip (5 mm, WPI) and sealed with dental acrylic. After the exposure was closed, the drainage hole was sealed with agarose. Fluorescein isothiocyanate (FITC)-labeled dextran (FD-2000S, Sigma) was injected intravenously (50–100 μl of 5 % (w/v) solution in saline) to visualize the vasculature and control for the integrity of the capillary bed.

In some experiments (n=4 subjects) Fluo-4 was used as a calcium indicator instead of OGB1. Fluo-4 (F-14201, Invitrogen, 50 μg) was prepared in the same way as OGB1 and applied topically for ~60 min, resulting in preferential labeling of astrocytes as previously described (Wang et al., 2006).

In experiments involving microinjection of drugs during imaging, the round coverslip was cut straight on one side. The cut side was aligned with the lateral edge of the exposure and a gap was left in the seal on the lateral side to allow insertion of a glass micropipette. ATP (A6419, Adenosine 5′-triphosphate disodium salt hydrate, Sigma), or t-ACPD (0187, (±)-1-Aminocyclopentane-*trans*-1,3-dicarboxylic acid, Tocris) was dissolved in ACSF, yielding 1-mM (ATP) or 10-μM (t-ACPD) drug solution. The blue fluorescent dye Alexa 350 (A-10439, Alexa Fluor 350 hydrazide, sodium salt, Invitrogen) was added to the drug solution so it would be possible to view the micropipette during manipulation and to provide visual feedback during microinjection (“puffing”) of the drug in the cortical tissue. The pressure was manually adjusted (~1–2 psi for 100 ms with a 2-μm pipette tip) to ensure visible puffs while avoiding movement artifacts.

During data acquisition, isoflurane was discontinued and anesthesia maintained with α-chloralose (50 mg*kg-1). Mice were paralyzed with pancuronium bromide 0.4 mg/kg/h (Shin et al., 2007) and ventilated (~110 bpm) with 30% O_2 in air. Expired CO_2 was measured continuously using a micro-capnometer (Cl240, Columbus instruments, Columbus, OH, USA). Heart rate, blood pressure, and body temperature were monitored continuously. In the majority of experiments, blood gas was analyzed to cross-validate the micro-capnometer measurements. Respiration was adjusted to achieve $PaCO_2$ between 30 and 40 mmHg and pH between 7.35 and 7.45. α-chloralose and pancuronium in 5% dextrose saline were supplied through the femoral line every 30 min for the duration of data acquisition.

Two-photon imaging

All measurements were performed in the forepaw region of SI. Imaging was done within a 1-mm radius from the center of the neuronal response, determined prior to the imaging session using surface potential recordings. Images were obtained using an Ultima two-

photon laser scanning microscopy system from Prairie Technologies equipped with an Ultra II femtosecond laser (Coherent) tuned to 790–1000 nm (790 nm in experiments with Alexa 350, 800–850 nm for calcium imaging with or without FITC, and up to 1000 nm for vascular FITC measurements). Green (OGB1 and FITC), red (SR101), and blue (Alexa 350) fluorophores were imaged using dedicated photodetectors: cooled GaAsP detectors for green and blue (Hamamatsu, H7422P-40), and a multialkali PMT for red (Hamamatsu, H7422-01). FITC and OGB1 have overlapping excitation and emission spectra and therefore can be excited together and imaged using the same (GaAsP) detector. This is possible because the signals separate in space: FITC is present only inside the intravascular lumen; OGB1, only in tissue.

We used a 4x objective (Olympus XLFluor4x/340, NA=0.28) to obtain low-resolution images of the exposure. Olympus 20x (XLUMPlanFI, NA=0.95) and Zeiss 40x (IR-ACHROPLAN, NA = 0.8) water-immersion objectives were used for high-resolution imaging. In experiments involving manipulation of a glass pipette under the coverslip, we used a combination of Zeiss 5x (Plan-NEOFLUAR, NA=0.16) and Olympus 20x (UMPlanFI, NA=0.5) objectives for a coarse approach and fine manipulation under the glass coverslip, respectively. The laser beam diameter was adjusted to overfill the back aperture.

For simultaneous calcium and vascular diameter measurements, a ~50×70-μm field-of-view (FOV) was imaged in frame-scan mode at the target acquisition rate of ~10 Hz, aiming to resolve 10% dilation of vessels with the baseline diameter of >8 μm. Additional diameter measurements were performed in frame-scan mode at ~10 Hz, or in a “free-hand” line-scan mode using ~1-mm-long line scans across multiple vessels with a scan rate of 80–170 Hz. The scan resolution was 0.5 μm or less.

No attempt was made to correct for optical aberrations resulting in elongation of the excitation volume along the depth axis (Ji et al., 2010). In OGB1 experiments, to prevent potential contamination of astrocytic signals from individual neuronal cell bodies outside the focal plane but within the axially stretched excitation volume, FOVs were chosen to ensure that no neuronal cell bodies were located immediately above or below the astrocytic cell bodies in the focal plane.

Stimulation

During electrical stimulation, a train of six 1-mA square 100-μs pulses at 3 Hz was delivered to the forepaw contralateral to the exposure through a pair of thin needles inserted under the skin. In OGB1 and Fluo-4 experiments, 10 and 3 stimulus trials, respectively, with interstimulus intervals (ISIs) of 25 s, were presented at each imaging location. This stimulus paradigm was chosen because it produced robust and reliable dilation, described in detail in our previous publications (Devor et al., 2008, Tian et al., 2010). Briefly, this stimulus induced a synchronized neuronal spiking response throughout the cortical depth within the center of the cortical forepaw representation (on the order of a millimeter across) and a temporally biphasic arteriolar diameter change with initial dilation followed by constriction. Within the center, the main vascular response was dilatory. The ratio of the amplitudes between the initial dilation and subsequent constriction decreased moving away from the center of neuronal activity (Devor et al., 2007). In the present study, two-photon measurements were restricted to the center region, thus ensuring robust dilation. Virtually every imaged neuron in the present study exhibited a stimulus-induced calcium increase. Similar behavior was observed in our recent study in the barrel cortex employing electrical stimulation of the whisker pad (Reznichenko et al., 2012).

During stimulation by microinjection of ATP or t-ACPD, the injecting micropipette was positioned using a Luigs & Neumann translation stage (380FM-U) and manipulation

equipment integrated into the Ultima system. Five to 10 puffs with ISIs of 50–80 s for ATP and 150–300 s for t-ACPD were presented at each imaging location.

Stimulation devices (A365 stimulus isolator or PV830 picopump, WPI) were triggered using a separate PC that also acquired timing signals for data acquisition ("trigger out" signals for each frame/line) and physiological readings using an National Instruments IO DAQ interface (PCI-6229) controlled by custom-written software in MATLAB (MathWorks, Inc.). The timing of each frame/line relative to the stimulus onset was determined during data analysis based on acquired triggering signals.

Extracellular electrophysiological recordings

In imaging experiments with calcium indicator Fluo-4, we employed simultaneous recordings of Multiple Unit Activity (MUA) to control for normal neuronal response to stimulation. This was necessary because neurons exhibited virtually no Fluo-4 uptake and, therefore, information about neuronal activity was not available from the calcium imaging data. MUA recordings were performed as described in (Devor et al., 2003, Devor et al., 2005), using a tungsten microelectrode (FHC, 7 MΩ) positioned ~200 μm below the cortical surface within the imaged column. The microelectrode was inserted under the coverslip as described above for glass pipettes. Because action potentials in neurons within ~100 μm of the electrode tip contribute to the MUA part of the extracellular potential (Buzsaki, 2004, Pettersen and Einevoll, 2008, Einevoll et al., 2012), the recorded signal mostly reflected spiking in layer II/III of the imaged cortical column.

Data analysis

Data were analyzed in MATLAB using custom-written software. Regions-of-interest (ROIs) corresponding to astrocytic cell bodies and perivascular endfeet were segmented from SR101 images. Neuronal cell bodies were segmented from composite red and green images. For individual ROIs, the calcium signal per frame was calculated as an average of all pixels within the ROI. This calculation was repeated for each frame in the time series to generate a single-ROI time-course. When more than one ROI per FOV was defined, the same procedure was performed separately for each ROI, resulting in a family of ROI-specific time-courses. When necessary, contamination from calcium increases in neuropil was regressed from astrocytic ROIs, as described in "Separation of astrocytic and neuropil signals" below.

Arteriolar ROIs were segmented at the outer border of the arteriolar wall. In the presence of FITC, dilation resulted in the expansion of fluorescent intravascular lumen within the ROI. The pixels within the intravascular core were brighter than the surrounding arteriolar wall; the diameter estimation procedure tracked the number of pixels above a threshold, separating the high-intensity intravascular lumen from the rest of the ROI.

Blood flow velocity in single arterioles was measured in the presence of intravascular FITC using repeated line scans (450–770 Hz for simultaneous diameter/velocity measurements and 1200–1700 Hz for dedicated velocity measurements) along the axis of the vessel. These formed a space-time image when stacked sequentially, leading to the generation of streaks due to the motion of red blood cells (Kleinfeld et al., 1998). The slope of these streaks is inversely proportional to the velocity, while the direction of flow is determined from the sign of the slope (Kleinfeld et al., 1998).

Ratio images were computed relative to the baseline image from a pre-stimulus time period with no spontaneous activity in either neuronal cell bodies or neuropil in the FOV; they included an average of 5 frames. All pixels outside astrocytic and vascular ROIs and neuronal cell bodies were specified as neuropil. Ratio images were calculated for each pixel

by (1) computing the difference in the signal intensity relative to the baseline image − ΔF, (2) dividing the ΔF by the baseline intensity − ΔF/F, and (3) multiplying the result by 100 to obtain the percent signal change.

Astrocytic calcium increases were detected when the intensity rose above the 2SD threshold relative to signal fluctuations within a 5-s pre-stimulus baseline and remained above the threshold for at least 5 consecutive time-points (~0.5 s). The onset was estimated by fitting a line to the rising slope between 20 and 80 % to the peak and calculating an intercept with the pre-stimulus baseline (Tian et al., 2010).

Statistics were performed across subjects unless indicated. The results were expressed as the mean±SE.

Separation of astrocytic and neuropil signals

Rationale—Since the volume occupied by astrocytic ROIs may contain neuronal processes (neuropil) (Halassa et al., 2007, Winship et al., 2007, Reeves et al., 2011), a calcium increase in the neuropil can contribute to the signal extracted from an astrocytic ROI defined from SR101 images. In fact, calcium signal increases within the first post-stimulus sampling interval, which are characteristic of neuropil response, were visible in all time-courses extracted from liberally defined “astrocytic” ROIs. The magnitude of this initial rapid transient decreased with decreases in the size of the astrocytic ROI (i.e., in astrocytic ROIs including less neuropil) and depended on the position of the focal plane relative to the astrocytic center of mass. Importantly, decreasing the size of the ROI selectively diminished the fast component, with neuropil kinetics preserving the delayed component when present (Fig. 1A–B). This fast component was a close replica of the time-course observed in the neuropil, and was composed of transients with a sharp rise and fast decay sufficient for resolving responses to each of the 6 stimuli in the train. Such a sharp rise is characteristic with neuronal calcium activity but has not been reported in astrocytes.

Moreover, calcium increases with neuropil-like kinetics were not observed in Fluo-4 experiments (Fig. 1C–D), in which the indicator was virtually absent in neurons. In these experiments, neuronal response was measured using simultaneous electrophysiological recordings (Fig. 1E). While in principle selective labeling of astrocytes eliminates the problem of cross-talk with neuronal calcium signals, astrocytic labeling with Fluo-4 was limited to the top 150–200 μm. In addition, in agreement with previous reports (Wang et al., 2006, Wang et al., 2009), labeled astrocytes exhibited increased sensitivity to laser power, raising concerns about a significant interference with normal tissue homeostasis associated with prolonged exposure to the Fluo-4 loading solution. Therefore, most of our results are based on OGB1 data where contamination from a calcium increase in the neuropil was minimized by decreasing the size of astrocytic ROIs and, in some cases, by using a linear regression approach as described in the following section.

Regression procedure—For OGB1 data, reducing the size of the ROI decreased the signal-to-noise ratio (SNR) of the measurement (compare the top and bottom red traces in Fig. 1B) and could result in underestimation of the number of responsive astrocytic trials. Therefore, in cases where the cross-talk could not be eliminated without compromising the SNR of the measurement (n=220 of the total of 619 astrocytes in WT subjects and n=30 of the total of 82 astrocytes in IP_3R2 subjects), we employed a linear regression approach. More formally, in MATLAB notation, we estimated the corrected astrocytic time-course as *x = y1 − y2*(y2|y1)*, where *y1* and *y2* were the observed astrocytic and neuropil time-courses, respectively. For each time-course extracted from an astrocytic ROI composed of *n* pixels, the corresponding neuropil time-course was estimated by averaging signal within a

ring of *n* neuropil pixels (excluding cell bodies) separated from the astrocytic ROI by a gap of the same area (that is, composed of *n* pixels).

Results

IP_3R2-KO mice lacking IP_3-dependent mechanism for astrocytic calcium increase have normal stimulus-induced vasodilation

We used *in vivo* two-photon microscopy for imaging of neuroglial calcium activity in the forepaw region of SI in IP_3R2-KO mice. Calcium indicator OGB1 and SR101 were used to label neurons (with OGB1) and astrocytes (with OGB1 and SR101) (Stosiek et al., 2003, Nimmerjahn et al., 2004, Garaschuk et al., 2006). In general agreement with previous studies that tested astrocytic IP_3-dependent calcium signaling in such mice (Petravicz et al., 2008, Di Castro et al., 2011, Takata et al., 2011, Navarrete et al., 2012, Thrane et al., 2012), we observed clear differences between IP_3R2-KO and WT subjects in the astrocytic response evoked by *in vivo* intracortical microinjection of ATP and a metabotropic glutamate receptor (mGluR) agonist t-ACPD (Fig. 2). ATP (1 mM) was presented at 3 cortical depths – in layer I, at the border between layers I and II, and in layer II – in 3 WT and 3 IP_3R2-KO subjects, producing a wave of astrocytic calcium increases in the former and no detectable response in the latter (Fig. 2A–D). The WT results agree with previously published *in vivo* observations of cerebellar Bergman glia (Hoogland et al., 2009) and a recent report on actrocytic signaling in the awake mouse cortex (Thrane et al., 2012).

Similarly, WT but not IP_3R2-KO subjects exhibited large-amplitude astrocytic calcium increases in response to 10 μM of t-ACPD. The drug was applied in 3 WT subjects (1 in layer I and 2 in layer II) and 4 IP_3R2-KO subjects (2 in layer I and 2 in layer II) (Fig. 2E–F). In contrast to our experience with ATP, we had to restrict application of t-ACPD to a single location per subject because safe repositioning of the pipette required application of positive pressure, leading to spillage of the drug. In WT subjects, spillage of t-ACPD induced irregular oscillations followed by a rapid decrease in responsiveness to successive puffs. For example, in a subject illustrated in Fig. 2E, time-locked calcium increases were observed in response to the first 3 puffs only. Astrocytic calcium oscillations following application of t-ACPD was previously observed *in vitro* (Fiacco and McCarthy, 2006). A decrease in t-ACPD efficiency during consecutive applications was also previously described in *vitro* and attributed by the authors to the depletion of intracellular calcium stores (Jaffe and Brown, 1994). This rapid and irreversible decrease in efficiency might explain an apparent disagreement of the present results with recent reports of t-ACPD at high concentrations (100–500 μM) failing to induce calcium increases in cultured astrocytes (Wang et al., 2012) or *in vivo* (Sun et al., 2013). In IP_3R2-KO subjects, we detected no change in astrocytic calcium in response to single puffs (Fig. 2F) or to an intentional spill using continuous low pressure for 1–2 min. Furthermore, astrocytes in IP_3R2-KO subjects did not exhibit detectable calcium increases in response to forepaw stimulation, in astrocytic cell bodies or perivascular endfeet (n=82 astrocytes and 34 endfeet imaged from the top of layer I to 210 μm below the surface; data not shown).

Next, we asked whether the lack of astrocytic calcium excitability in IP_3R2-KO mice had an effect on sensory stimulus-induced vascular response. To address this question, we measured arteriolar vasodilation in 6 WT subjects and 3 IP_3R2-KO subjects in response to the forepaw stimulus. Diving arterioles, labeled with intravascular FITC, were traced from the surface. The identity of the imaged vessels was verified at the end of each experiment by acquiring high-resolution image stacks. Fig. 3A shows a compilation of individual vasodilation time-courses for the WT (top) and KO (bottom) populations. The onset of vasodilation was estimated by fitting a line to the rising slope of the diameter increase and calculating an intercept with the pre-stimulus baseline (Tian et al., 2010). The extracted

onset and peak distributions (Fig. 3B, top and bottom plots, respectively) for the WT and KO populations (solid circles and open triangles, respectively) overlapped. There was no statistically significant cross-subject difference between the WT and KO results: Averaged within the top 550 μm, vasodilation started 0.8±0.1 and 0.6±0.5 s and peaked 3.2±0.2 and 3±0.2 s from the stimulus onset in WT and IP_3R2-KO populations, respectively. The relatively rapid dilation onsets are in agreement with recent single-vessel imaging studies by us and by others (Tian et al., 2010, Drew et al., 2011, Schulz et al., 2012, Shen et al., 2012).

To confirm that an increase in arteriolar diameter was indicative of an increase in cerebral blood flow, we performed paired diameter and red blood cell velocity measurements (see **Materials and Methods**) – either simultaneously or sequentially – for 15 surface arterioles in an additional 4 WT subjects. These measurements demonstrated that an increase in arteriolar diameter was consistently accompanied by an increase in blood flow velocity (Fig. 3C–D). Thus, increase in diameter can be used as a surrogate measure of functional hyperemia.

Taken together, these results show that elevation of astrocytic calcium was not required for normal functional hyperemia in IP_3R2-KO mice.

Astrocytes may exhibit sporadic calcium increases in the presence of robust neuronal response and vasodilation

After establishing that IP_3R2-KO mice exhibit normal functional hyperemia, we proceeded to investigate the relationship between astrocytic increases in intracellular calcium and vasodilation in WT mice in response to forepaw stimulation. Similar to our previous studies in rats (Devor et al., 2008, Tian et al., 2010), this stimulus elicited reproducible dilation (Fig. 3), which was then used as a reference in addressing the question: *given the dilation*, can we detect a preceding astrocytic calcium increase? We performed simultaneous imaging of neuroglial calcium activity and arteriolar vasodilation at different depths in 6 WT subjects: from the top of layer I to 410 μm below the surface. Diving arterioles were included in 142 FOVs and capillaries >100 μm away from arterioles – in 113 FOVs. Six additional WT subjects were used for calcium imaging only.

Each FOV, which included one or more astrocytic cell bodies, was imaged continuously for ~260 s during presentation of 10 stimulus trials. A significant increase in astrocytic intracellular calcium (>2SD, see **Materials and Methods**) with an onset within a 6-s window following the stimulus onset was considered a stimulus-induced "astrocytic calcium response." Of the total of 619 astrocytes imaged in 12 subjects from the surface (the top of layer I) to 410 μm below the surface (layer IV (Anderson et al., 2009)), the majority (90±3%), exhibited no astrocytic calcium response within the 6-s window during any of the stimulus trials, despite a robust neuronal response and vasodilation. An example FOV with an arteriole diving through the imaging plane and one perivascular astrocyte is shown in Fig. 4. The arteriole (Fig. 4A, "v" stands for "vessel") was labeled by intravascular injection of FITC. The signal time-course extracted from the astrocytic ROI (Fig. 4A, "a1") exhibited no change in response to any of the stimulus trials (the red trace in Fig. 4B). In contrast, clear calcium increases were observed in neuronal cell bodies (Fig. 4B, "n1" to "n3," green traces). A robust calcium increase was also detected in the neuropil (the bottom green trace in Fig. 4B).

The arteriolar diameter increased in response to each stimulus trial (the black trace in Fig. 4B). The lack of astrocytic calcium increase in the presence of arteriolar dilation and neuronal response can also be seen in ratio images, which illustrate the percent change in fluorescence relative to the pre-stimulus baseline ($\Delta F/F$, see **Materials and Methods**) for the first stimulus trial (Fig. 4C). Dilation of the arteriole in the ratio images appeared as a

bright ring, indicating the expansion of FITC-labeled intravascular lumen. The signal within the astrocytic ROI, located outside the dilation ring (see ROI contours overlaid on the ratio images), remained at the baseline. The same dilation is illustrated in Fig. 4D through a comparison of "raw" images: at the pre-stimulus baseline (top) and during the peak dilation (bottom). The dilation is visible as an expansion of the intravascular cross-section relative to the baseline diameter indicated by the red dotted line.

At high enough concentrations, the presence of calcium indicator can slow the kinetics of calcium rise and attenuate the response amplitude. To control for this unwanted effect, which would apply to both astrocytes and neurons, we estimated a time constant of neuronal calcium decay using established procedures (Gobel and Helmchen, 2007). Consistent with previous studies estimating neuronal spikes from two-photon calcium imaging data, neuronal calcium transients extracted from cell body ROIs decayed with a time constant of 0.5–0.9 s (Fig. 4E). Thus, our measurements were performed within a range of intracellular OGB1 concentrations where the presence of indicator molecules did not considerably alter cellular calcium kinetics.

Cortical layer boundaries were defined by depth (Anderson et al., 2009). In layer II/III (100–320 μm), 13±4% of astrocytes responded to at least 1 stimulus trial. This is in contrast to layer I (<100 μm) and layer IV (320–410 μm), where only a few astrocytes exhibited calcium responses: 2 cells (of 166) in layer I and 3 cells (of 94) in layer IV. Taken together, these numbers correspond to ~7% of the astrocytes from the overall pool of 619 responding to at least 1 stimulus trial. The most responsive cases from our pool exhibited astrocytic calcium elevations in a number of consecutive trials, similar to previously published results (Wang et al., 2006, Wang et al., 2009, Thrane et al., 2012) (Fig. 1B). However, the majority of the responsive astrocytes responded sporadically to only a few trials: an average of 2 of 10 trials. Fig. 5 shows an example where calcium increases in response to 2 of 10 trials were observed in one of 3 astrocytes in the FOV ("a1," Fig. 5A). Small-amplitude "spikes", time-locked to the stimulus onset, are visible on astrocytic time-courses in some of the trials in Fig. 5B, representing a residual cross-talk with neuropil signals (see **Materials and Methods**, "Separation of astrocytic and neuropil signals"). To illustrate this effect in a more intuitive way, we calculated a series of trial-averaged ratio images during the neuronal response (Fig. 5C). While the astrocytic ROIs stayed darker than the surrounding neuropil, their outer borders brightened during signal increases in the neuropil. This is in contrast to the responses in trials 2 and 9 (red arrows in Fig. 5B) where the signal increase was clearly confined to the astrocytic ROI. This is illustrated in Fig. 5D through a series of ratio images corresponding to trial 9. These images are spaced in time (times are indicated above the images) to optimize the visualization of slow astrocytic calcium kinetics. In contrast to astrocytes, all neuronal cell bodies and neuropil reliably responded, with an increase in calcium, to every stimulus trial (Fig. 5B–C).

Next, we examined whether the responsive astrocytes (i.e., those responding to at least one stimulus trial) were unique in their geometrical position relative to the target blood vessels. Based on published anatomical data, we assumed that the processes of a single astrocyte (the "astrocytic domain") in the mouse cortex extended roughly up to 50 μm from the cell body (Halassa et al., 2007). Using this assumption, we divided astrocytes imaged in FOVs that included diving arterioles (n=142 FOVs) into those with cell bodies within 50 μm of an arteriole (Fig. 6A) and those with cell bodies at a distance greater than 50 μm – presumably in contact with capillaries or venules (Fig. 6B). All astrocytes from FOVs within the capillary bed (n=113 FOVs) were assigned to the > 50 μm category. On average, astrocytes that responded to at least one stimulus trial were more frequently found near arterioles (16±6%) than outside the 50 μm (7±4%). However, this difference was not statistically significant across subjects. The time-courses of astrocytic calcium responses from these 2

categories did not differ significantly, although those near arterioles exhibited a small trend toward an earlier onset, earlier peak, and shorter duration (Fig. 6C).

The onset of astrocytic calcium response may lag behind the onset of vasodilation

The sporadic occurrence of calcium response in individual astrocytes, on its own, does not rule out their involvement in triggering vasodilation. In principle, calcium-dependent release of gliotransmitters from a few cells along a target arteriole might be sufficient to initiate dilation. However, if vasodilation is triggered by astrocytes via an intracellular pathway that requires an increase in cytosolic calcium, the onset of an astrocytic calcium response must precede that of vasodilation. To test this temporal relationship, we compared time-courses of astrocytic calcium increase and arteriolar dilation (Fig. 7).

Because our measurements indicated that only a small percentage of astrocytes exhibited a calcium response in each individual subject, we collected all responsive stimulus trials – across astrocytes and subjects – for quantitative analysis. Fig. 7A shows a compilation of astrocytic calcium time-courses from the responsive trials separately for the subjects with intravascular FITC used for simultaneous measurements of dilation (n=6 subjects, left panel) and without FITC (n=6 subjects, right panel). The average time-courses for these 2 categories overlapped (Fig. 7A, inset) and data were pooled together for quantitative analysis, including 73 trials from 31 cell body ROIs and 15 trials from 5 endfeet ROIs. For each responsive trial, we estimated the onset by fitting a line to the rising slope of the signal and calculating an intercept with the pre-stimulus baseline (Tian et al., 2010). Duration was estimated as the full width of the response at half maximum amplitude (FWHM). On average, the onset and peak of astrocytic calcium increase were delayed by 3.6±1.2 and 8.1±3.3 s, respectively, from the stimulus onset. These calcium increases exhibited an amplitude of 16.8±10.8 % ($\Delta F/F$) and a duration of 6.6±4.1 s (mean±SD across all responsive trials). Astrocytic onset and time-to-peak values for all responsive stimulus trials in our dataset are shown in Fig. 7B (top and bottom, respectively) as a function of the cortical depth (red open squares: subjects with FITC; red solid dots: subjects without FITC). The 3.6-s onset is in good agreement with the onset recently reported for whisker stimulation in the awake mouse (~3.5 s) and faster than that observed under other types of anesthesia (~5.7 s under ketamine/xylazine, isoflurane, or urethane) in the same study (Thrane et al., 2012), suggesting less suppressive effects of α-chloralose on astrocytic calcium kinetics.

The onset of vasodilation was estimated in the same way as the onset of astrocytic calcium response: by fitting a line to the rising slope of the diameter increase and calculating an intercept with the pre-stimulus baseline (Tian et al., 2010). The extracted vascular values are shown in Fig. 7B (black symbols). Simultaneously measured diameters (Fig. 7B, black open squares) are included regardless of the presence of an astrocytic calcium response. Superposition of onset and peak values from the stand-alone arteriolar diameter measurements in the absence of additional fluorophores (OGB1 and SR101) in WT mice (Fig. 7B, black solid dots) confirmed that the kinetics of the vascular measurements acquired simultaneously with calcium imaging were representative of arterioles in the corresponding depth category. The same stand-alone arteriolar diameter data are illustrated in solid black dots in Fig. 3.

The distribution of astrocytic onset times in Fig. 7B falls above that of dilation, indicating that astrocytic calcium increases lagged behind the onset of dilation across the cortical depths considered. The difference between astrocytic and dilation kinetics is further illustrated in Fig. 7C, which compares the overall pool of astrocytic response time-courses (combined from the 2 plots in Fig. 7A) with vasodilation (combined simultaneous and stand-alone data). On average, the onset of astrocytic calcium responses was delayed from that of

dilation by >2 s: the astrocytic and vascular onsets were 3.6±1.2 and 0.7±0.4 s, respectively (mean±SD across all measurements). Similarly, the time-to-peak of astrocytic calcium response was delayed relative to that of dilation (8.1±3.3 and 3.3±0.7 s, respectively, mean ±SD across all measurements).

Sub-cellular compartment-specificity of astrocytic calcium transients: perivascular endfeet and fine astrocytic processes

It has been reported that the onset of calcium increase in astrocytic perivascular endfeet, *in vivo,* can precede that in the cell body (Wang et al., 2006). We therefore examined 43 cases (from the WT population) where an astrocytic cell body had a connected endfoot in the same imaging plane (within the same FOV). Of these, 35 exhibited no detectable elevation of calcium in either the cell body or the endfoot compartment, while 3 exhibited elevation in the cell body but not in the endfoot. In the remaining 5 cases, both compartments showed an increase – including 3 cases in which the onset of a calcium response in the endfoot preceded that in the soma. One of these is illustrated in Fig. 8A–D: Here, both the soma and endfoot ("a1" and "EF" in Fig. 8A) responded to the seventh stimulus trial with a large-amplitude calcium increase (the red arrowhead points to the endfoot response). As in Fig. 5, small-amplitude "spikes" at the beginning of some of the stimulus trials reflect residual cross-talk with neuropil signals (see **Materials and Methods**, "Separation of astrocytic and neuropil signals"). This can be seen in trial-averaged ratio images during the neuronal response, in which astrocytic ROIs remained darker than the surrounding neuropil (Fig. 8C). Ratio images for the seventh stimulus trial in Fig. 8D show that calcium increases occurred not only in the soma and endfoot but also in fine astrocytic processes around the soma – compare the 12–13 s post-stimulus ratio image in Fig. 8D to the SR101 image in Fig. 8A. In addition to the high-amplitude response, small-amplitude trends were observed in the endfoot in the first 3 stimulus trials (black arrowheads). These trends did not cross the 2SD threshold for detection of astrocytic responses (see **Materials and Methods**). Superposition of these trends with the high-amplitude endfoot response in Fig. 8E suggested similar onsets. All of the detected endfoot responses (n=15 trials, 5 endfeet) are overlaid in Fig. 8F. The onset of the endfoot calcium increase was delayed relative to the mean dilation onset in the same depth category (180–300 μm, the black trace): 2.6±0.6 and 0.8±0.3 s, respectively (mean±SD across all time-courses). The same endfoot responses are included in the <50 μm category in Fig. 6 and in the overall pool of detected astrocytic responses in Fig. 7.

The increases in intracellular calcium in astrocytic processes that are visible in the ratio images in Fig. 8D argue for our ability to detect sub-cellular transients. However, non-specific labeling of all cells in the volume by OGB1 presents a challenge in isolating calcium signals from the fine astrocytic arborizations. Moreover, astrocytic cell bodies can be porous and contain neuronal processes, thus necessitating in some cases regression of the neuropil signal from astrocytic ROIs (see **Materials and Methods**, "Separation of astrocytic and neuropil signals"). Therefore, as long as the indicator is present in both neurons and astrocytes, the existence of neuropil-like astrocytic calcium kinetics cannot be completely ruled out. In particular, a hypothetical astrocytic calcium elevation that exhibits a smaller amplitude than the elevation in the surrounding neuropil and that has kinetics identical to those in the neuropil could be erroneously removed from the astrocytic time-course by the regression procedure. We therefore employed a topical loading of Fluo-4 in an additional 4 subjects, with the goal of examining astrocytic calcium kinetics and sub-cellular organization of astrocytic calcium increases within a limited range of cortical depths achievable with topical loading. The topical loading procedure resulted in uptake by astrocytes but not by neurons (Wang et al., 2006). Sub-cellular ROIs in these experiments were defined by thresholding maximal intensity projection (MIP) images computed for each stimulus trial. Care was taken to choose a baseline image with no spontaneous activity. In

addition to large-amplitude calcium increases in astrocytic cell bodies and perivascular endfeet, similar to those observed with OGB1, Fluo-4-labeled astrocytes exhibited patchy calcium increases that did not co-localize with cell bodies (Fig. 9A–B). These calcium changes were slow compared with those in neurons and neuropil (from the OGB1 data, e.g., the green traces in Fig. 4–5) and could occur in the absence of a concomitant calcium increase in the cell body, in agreement with a recent high-resolution study of hippocampal astrocytes in a brain slice preparation (Di Castro et al., 2011). Limited by the sensitivity and resolution of our measurements, we did not attempt to address whether some of the calcium rises within individual sub-cellular ROIs could be considered stimulus-induced. However, in some cases (14 of 51 FOVs) we could detect a repeatable stimulus-locked calcium increase in at least 2 of the 3 trials, presented at each FOV in Fluo-4 experiments, by averaging all pixels within the FOV ("field response," the blue trace in Fig. 9C). Fig. 9D compares the time-course of Fluo-4 field response to that of calcium increases in astrocytic cell bodies and vasodilation within the depth range of Fluo-4 measurements. The onset of the averaged field response (averaged across the 14 FOVs, the blue trace in Fig. 9D) preceded that of the averaged calcium response in astrocytic cell bodies (the red trace in Fig. 9D) but lagged behind that of vasodilation (the black trace in Fig. 9D).

Discussion

Collectively, our results demonstrate the following: (1) no astrocytic calcium increase was needed for a normal vasodilation response in IP_3R2-KO mice; (2) calcium increases in astrocytic cell bodies and perivascular endfeet, evoked by an increase in neuronal activity in response to a short-duration sensory stimulus, were too slow in the onset to initiate vasodilation; and (3) astrocytic calcium increases were observed in a small population of astrocytes sporadically responding to individual stimulus trials. These findings challenge the view that astrocytes relay the increase in local neuronal activity to vascular contractile elements via calcium-dependent mechanisms. In particular, the temporal order of events – with the onset of the astrocytic calcium response lagging behind that of arteriolar dilation – may indicate that vasodilation cannot be triggered by any process downstream from the increase in astrocytic cytosolic calcium.

Comparison with previous studies

The average onset of astrocytic calcium increase at >1 s following the stimulus onset observed here is in agreement with the general consensus based on previous *in vivo* reports in the primary sensory and visual cortices: ~ 3 s has been reported in the mouse SI for whisker stimulation (Wang et al., 2006, Wang et al., 2009, Thrane et al., 2012), >4 s in the rat SI for electrical forepaw stimulation (Schulz et al., 2012), 3–4 s in the visual cortex of ferrets (Schummers et al., 2008), and 1–2 s in the mouse SI after the onset of voluntary running (Dombeck et al., 2007). Although neither of these specifically addressed the existence of astrocytic calcium increases prior to dilation onset, Schultz et al. (2012) noted instances of vasodilation in the absence of astrocytic calcium increases. In addition, an indication of a temporal discrepancy between vasodilation and astrocytic calcium is found in Schummers et al. (2008) where intrinsic signal change, related to vasodilation, occurred prior to the onset of the astrocytic calcium increase (~1 and 3 s, in their Fig. 4E and 4B, respectively).

Simultaneous measurements of glial calcium and blood flow were performed in the olfactory bulb (Petzold et al., 2008) and cerebellum (Nimmerjahn et al., 2009). While Petzold et al. (2008) did not specifically determine the onsets, our present conclusions are in agreement with a more recent overview by the same authors, which states that "astrocytic responses *in vivo* are typically detected after the onset of functional hyperemia" (Petzold and Murthy, 2011). Nimmerjahn et al. (2009) reported that "local blood perfusion levels

rose over a very similar time course as that of Ca^{2+} flares" in cerebellar Bergman glia (their Fig. 7C). Thus, calcium excitability and the kinetics of calcium surges can differ between glial subtypes across brain regions.

A single study by Winship et al. (2007) reported that ~ 5 % of imaged astrocytes exhibited fast calcium signals with the onset indistinguishable from that of neurons (Winship et al., 2007) (see their Fig. 2). This type of behavior has not been reproduced in any subsequent studies. While the quest to find astrocytes with neuronal-like calcium kinetics continues, it is possible that those observed in Winship et al. were misclassified neurons or "bleed-through" from strongly responsive neurons positioned immediately under the focal plane (Ji et al., 2010).

A sporadic and late appearing of astrocytic calcium response is in apparent disagreement with the rapid and reproducible kinetics of astrocytic glutamate transporter (Bergles and Jahr, 1997). An increase in intracellular calcium, however, has not been established as a necessary consequence of the transporter's activation (Petzold et al., 2008). Therefore, the lack of calcium increase should not be interpreted as astrocytes' inability to sense neuronal activation. In fact, astrocytes are known to respond to neuronal activation by increased metabolic activity, upregulation of glutamate-glutamine shuttle, and glucose uptake (Allaman et al., 2011, Pellerin and Magistretti, 2012). The current data suggest that these astrocytic functions are not necessarily accompanied by calcium increases.

The hypothesis that astrocytic calcium increases mediate neurovascular coupling was originally put forward in studies in brain slices (Zonta et al., 2003, Mulligan and MacVicar, 2004, Metea and Newman, 2006). However, the pathological homeostasis of brain slices departs from that *in vivo* (Turner et al., 2007, Huchzermeyer et al., 2008). More recently, the hypothesis gained support from an *in vivo* study in which photolysis ("uncaging") of caged glutamate induced dilation of diving cerebral arterioles (Takano et al., 2006). With the caveat that single-photon uncaging could result in the uncaging of calcium in astrocytic and neuronal elements above and below the focal plane, this study supports the conclusion that astrocytes house a machinery to synthesize and release vasoactive substances upon calcium increase. The present study does not contradict this conclusion. Rather, we show that a stimulus-induced increase in neuronal activity may not set off that machinery fast enough to account for the onset of vasodilation.

Sub-cellular calcium transients and limitations of the bulk loading method

In agreement with earlier observations in the SI (Wang et al., 2006), in some instances the onset of calcium increases in perivascular endfeet preceded that in the cell body. Our Fluo-4 data further support the idea of sub-cellular organization of astrocytic calcium activity, suggesting that local increases in astrocytic arborizations are independent of those in cell bodies. However, the onset of calcium increases in perivascular endfeet and that of the field response in Fluo-4 data lagged behind the onset of vasodilation.

It has been demonstrated in cell cultures that membrane-bound genetic calcium indicators can have superior performance to cytoplasmic dyes (such as OGB1 and Fluo-4, which were used in the present study) in detecting local calcium rises under the membrane (Shigetomi et al., 2010a, Shigetomi et al., 2010b, Shigetomi et al., 2011). Translation of this technology *in vivo* is under development but is not yet available. As an alternative strategy, we employed IP_3R2-KO mice (Li et al., 2005, Petravicz et al., 2008), which lack the IP3-dependent mechanism for astrocytic calcium increase but show normal vasodilation. This finding is consistent with a recent report demonstrating that blocking mGluR type 5 (mGluR5) upstream of the IP_3-dependent calcium release from intracellular stores did not affect the hemodynamic response to a brief sensory stimulus (Calcinaghi et al., 2011). We cannot rule

out, however, potential IP_3-independent fast calcium increases in astrocytic "microdomains" below the detection ability of Fluo-4 imaging. IP_3-independent calcium influx – mediated by transient receptor potential A1 channels – has been shown in astrocytic cultures (Shigetomi et al., 2011); the contextual relevance for this mechanism *in vivo* remains an open question.

Future technological developments aimed at improving the sensitivity of two-photon detection and targeted expression of novel genetically induced calcium indicators might lead to the discovery of possible fast sub-cellular astrocytic calcium surges powering a timely release of vasoactive gliotransmitters *in vivo*. Thus far, however, the evidence used to support the hypothesis of an astrocytic role in triggering vasodilation has been based on calcium signals detectable with the currently available two-photon calcium imaging technology, such as that used in the present study. Our simultaneous measurements demonstrate that these astrocytic calcium signals may not explain the onset of vasodilation.

Additional limitations of the present study

Our experiments were performed in the presence of a paralytic agent and general anesthesia; the latter has been shown to modulate astrocytic calcium response (Schummers et al., 2008, Nimmerjahn et al., 2009, Thrane et al., 2012). While anesthesia can differentially affect astrocytic activity, delayed astrocytic calcium responses were observed in our study *in the presence of robust arteriolar vasodilation*. Thus, under our experimental conditions, an increase in astrocytic calcium was not required for triggering vasodilation.

A decrease of SNR with depth in two-photon measurements could account for the few astrocytic calcium responses in layer IV detected in the present study. In addition, since layers V and VI were not sampled, we cannot rule out the possibility of faster astrocytic calcium responses in these layers.

Remaining questions

While our findings suggest that healthy hyperemia in response to a brief stimulus might not rely on gliotransmitters, the mechanism for regulation of vascular (arteriolar and capillary) diameters remains an open question. Similarly, the biological relevance of astrocytic calcium transients requires further investigation. What messengers mediate neurovascular communication in the healthy brain (Cauli and Hamel, 2010, Lecrux et al., 2011), and how do they reach contractile vascular elements largely covered by astrocytic endfeet? What physiological or pathophysiological conditions set off the astrocytic machinery for synthesis and release of vasodilators and constrictors *in vivo*? Do astrocytes play a role in maintaining dilation during sustained elevation of neuronal activity (Shi et al., 2008, Schulz et al., 2012) or in matching cerebral perfusion to different levels of neuronal activity associated with different brain rhythms (Steriade, 2006)? Does the biological relevance of astrocytic calcium transients lie outside the realm of neurovascular research, e.g., in the regulation of neuronal excitability (Di Castro et al., 2011, Poskanzer and Yuste, 2011) or in gene transcription related to the maintenance of tissue homeostasis? Future *in vivo* studies will provide answers to these questions and thus pave the way for deciphering the enigma of astrocytic function and neurovascular communication.

Acknowledgments

We gratefully acknowledge support from the NINDS (NS051188 and NS057198 to AD, NS057476 and NS055104 to DAB, NS054736 to GAS) and NIBIB (EB00790 to AMD and EB009118 to AD), AHA (11SDG7600037 to SS) and European Regional Development Fund (CEITEC (CZ.1.05/1.1.00/02.0068) to HU).

References

Agulhon C, Petravicz J, McMullen AB, Sweger EJ, Minton SK, Taves SR, Casper KB, Fiacco TA, McCarthy KD. What is the role of astrocyte calcium in neurophysiology? Neuron. 2008; 59:932–946. [PubMed: 18817732]

Allaman I, Belanger M, Magistretti PJ. Astrocyte-neuron metabolic relationships: for better and for worse. Trends Neurosci. 2011; 34:76–87. [PubMed: 21236501]

Anderson LA, Christianson GB, Linden JF. Mouse auditory cortex differs from visual and somatosensory cortices in the laminar distribution of cytochrome oxidase and acetylcholinesterase. Brain Res. 2009; 1252:130–142. [PubMed: 19061871]

Attwell D, Buchan AM, Charpak S, Lauritzen M, Macvicar BA, Newman EA. Glial and neuronal control of brain blood flow. Nature. 2010; 468:232–243. [PubMed: 21068832]

Bergles DE, Jahr CE. Synaptic activation of glutamate transporters in hippocampal astrocytes. Neuron. 1997; 19:1297–1308. [PubMed: 9427252]

Boas DA, Jones SR, Devor A, Huppert TJ, Dale AM. A vascular anatomical network model of the spatio-temporal response to brain activation. Neuroimage. 2008; 40:1116–1129. [PubMed: 18289880]

Buzsaki G. Large-scale recording of neuronal ensembles. Nat Neurosci. 2004; 7:446–451. [PubMed: 15114356]

Calcinaghi N, Jolivet R, Wyss MT, Ametamey SM, Gasparini F, Buck A, Weber B. Metabotropic glutamate receptor mGluR5 is not involved in the early hemodynamic response. J Cereb Blood Flow Metab. 2011; 31:e1–10. [PubMed: 21731033]

Cauli B, Hamel E. Revisiting the role of neurons in neurovascular coupling. Front Neuroenergetics. 2010; 2:9. [PubMed: 20616884]

Devor A, Dunn AK, Andermann ML, Ulbert I, Boas DA, Dale AM. Coupling of total hemoglobin concentration, oxygenation, and neural activity in rat somatosensory cortex. Neuron. 2003; 39:353–359. [PubMed: 12873390]

Devor A, Hillman EM, Tian P, Waeber C, Teng IC, Ruvinskaya L, Shalinsky MH, Zhu H, Haslinger RH, Narayanan SN, Ulbert I, Dunn AK, Lo EH, Rosen BR, Dale AM, Kleinfeld D, Boas DA. Stimulus-induced changes in blood flow and 2-deoxyglucose uptake dissociate in ipsilateral somatosensory cortex. J Neurosci. 2008; 28:14347–14357. [PubMed: 19118167]

Devor A, Tian P, Nishimura N, Teng IC, Hillman EM, Narayanan SN, Ulbert I, Boas DA, Kleinfeld D, Dale AM. Suppressed neuronal activity and concurrent arteriolar vasoconstriction may explain negative blood oxygenation level-dependent signal. J Neurosci. 2007; 27:4452–4459. [PubMed: 17442830]

Devor A, Ulbert I, Dunn AK, Narayanan SN, Jones SR, Andermann ML, Boas DA, Dale AM. Coupling of the cortical hemodynamic response to cortical and thalamic neuronal activity. Proc Natl Acad Sci U S A. 2005; 102:3822–3827. [PubMed: 15734797]

Di Castro MA, Chuquet J, Liaudet N, Bhaukaurally K, Santello M, Bouvier D, Tiret P, Volterra A. Local Ca2+ detection and modulation of synaptic release by astrocytes. Nat Neurosci. 2011; 14:1276–1284. [PubMed: 21909085]

Dombeck DA, Khabbaz AN, Collman F, Adelman TL, Tank DW. Imaging large-scale neural activity with cellular resolution in awake, mobile mice. Neuron. 2007; 56:43–57. [PubMed: 17920014]

Drew PJ, Shih AY, Kleinfeld D. Fluctuating and sensory-induced vasodynamics in rodent cortex extend arteriole capacity. Proc Natl Acad Sci U S A. 2011; 108:8473–8478. [PubMed: 21536897]

Einevoll GT, Franke F, Hagen E, Pouzat C, Harris KD. Towards reliable spike-train recordings from thousands of neurons with multielectrodes. Curr Opin Neurobiol. 2012; 22:11–17. [PubMed: 22023727]

Fiacco TA, McCarthy KD. Astrocyte calcium elevations: properties, propagation, and effects on brain signaling. Glia. 2006; 54:676–690. [PubMed: 17006896]

Garaschuk O, Milos RI, Konnerth A. Targeted bulk-loading of fluorescent indicators for two-photon brain imaging in vivo. Nature protocols. 2006; 1:380–386.

Gobel W, Helmchen F. In vivo calcium imaging of neural network function. Physiology (Bethesda). 2007; 22:358–365. [PubMed: 18073408]

Gordon GR, Choi HB, Rungta RL, Ellis-Davies GC, MacVicar BA. Brain metabolism dictates the polarity of astrocyte control over arterioles. Nature. 2008; 456:745–749. [PubMed: 18971930]

Halassa MM, Dal Maschio M, Beltramo R, Haydon PG, Benfenati F, Fellin T. Integrated brain circuits: neuron-astrocyte interaction in sleep-related rhythmogenesis. Scientific World Journal. 2010; 10:1634–1645. [PubMed: 20730381]

Halassa MM, Fellin T, Takano H, Dong JH, Haydon PG. Synaptic islands defined by the territory of a single astrocyte. J Neurosci. 2007; 27:6473–6477. [PubMed: 17567808]

Hoogland TM, Kuhn B, Gobel W, Huang W, Nakai J, Helmchen F, Flint J, Wang SS. Radially expanding transglial calcium waves in the intact cerebellum. Proc Natl Acad Sci U S A. 2009; 106:3496–3501. [PubMed: 19211787]

Huchzermeyer C, Albus K, Gabriel HJ, Otahal J, Taubenberger N, Heinemann U, Kovacs R, Kann O. Gamma oscillations and spontaneous network activity in the hippocampus are highly sensitive to decreases in pO2 and concomitant changes in mitochondrial redox state. J Neurosci. 2008; 28:1153–1162. [PubMed: 18234893]

Iadecola C, Nedergaard M. Glial regulation of the cerebral microvasculature. Nat Neurosci. 2007; 10:1369–1376. [PubMed: 17965657]

Jaffe DB, Brown TH. Metabotropic glutamate receptor activation induces calcium waves within hippocampal dendrites. J Neurophysiol. 1994; 72:471–474. [PubMed: 7965030]

Ji N, Milkie DE, Betzig E. Adaptive optics via pupil segmentation for high-resolution imaging in biological tissues. Nat Methods. 2010; 7:141–147. [PubMed: 20037592]

Kleinfeld D, Mitra PP, Helmchen F, Denk W. Fluctuations and stimulus-induced changes in blood flow observed in individual capillaries in layers 2 through 4 of rat neocortex. Proc Natl Acad Sci U S A. 1998; 95:15741–15746. [PubMed: 9861040]

Koehler RC, Roman RJ, Harder DR. Astrocytes and the regulation of cerebral blood flow. Trends Neurosci. 2009; 32:160–169. [PubMed: 19162338]

Lecrux C, Toussay X, Kocharyan A, Fernandes P, Neupane S, Levesque M, Plaisier F, Shmuel A, Cauli B, Hamel E. Pyramidal neurons are “neurogenic hubs” in the neurovascular coupling response to whisker stimulation. J Neurosci. 2011; 31:9836–9847. [PubMed: 21734275]

Li X, Zima AV, Sheikh F, Blatter LA, Chen J. Endothelin-1-induced arrhythmogenic Ca2+ signaling is abolished in atrial myocytes of inositol-1,4,5-trisphosphate(IP3)-receptor type 2-deficient mice. Circ Res. 2005; 96:1274–1281. [PubMed: 15933266]

Magistretti PJ, Pellerin L, Rothman DL, Shulman RG. Energy on demand. Science. 1999; 283:496–497. [PubMed: 9988650]

Metea MR, Newman EA. Glial cells dilate and constrict blood vessels: a mechanism of neurovascular coupling. J Neurosci. 2006; 26:2862–2870. [PubMed: 16540563]

Mulligan SJ, MacVicar BA. Calcium transients in astrocyte endfeet cause cerebrovascular constrictions. Nature. 2004; 431:195–199. [PubMed: 15356633]

Navarrete M, Perea G, Fernandez de Sevilla D, Gomez-Gonzalo M, Nunez A, Martin ED, Araque A. Astrocytes mediate in vivo cholinergic-induced synaptic plasticity. PLoS Biol. 2012; 10:e1001259. [PubMed: 22347811]

Nimmerjahn A. Astrocytes going live: advances and challenges. J Physiol. 2009; 587:1639–1647. [PubMed: 19204050]

Nimmerjahn A, Kirchhoff F, Kerr JN, Helmchen F. Sulforhodamine 101 as a specific marker of astroglia in the neocortex in vivo. Nat Methods. 2004; 1:31–37. [PubMed: 15782150]

Nimmerjahn A, Mukamel EA, Schnitzer MJ. Motor behavior activates Bergmann glial networks. Neuron. 2009; 62:400–412. [PubMed: 19447095]

Paulson OB, Hasselbalch SG, Rostrup E, Knudsen GM, Pelligrino D. Cerebral blood flow response to functional activation. J Cereb Blood Flow Metab. 2010; 30:2–14. [PubMed: 19738630]

Pellerin L, Magistretti PJ. Sweet sixteen for ANLS. J Cereb Blood Flow Metab. 2012; 32:1152–1166. [PubMed: 22027938]

Petravicz J, Fiacco TA, McCarthy KD. Loss of IP3 receptor-dependent Ca2+ increases in hippocampal astrocytes does not affect baseline CA1 pyramidal neuron synaptic activity. J Neurosci. 2008; 28:4967–4973. [PubMed: 18463250]

Pettersen KH, Einevoll GT. Amplitude variability and extracellular low-pass filtering of neuronal spikes. Biophys J. 2008; 94:784–802. [PubMed: 17921225]

Petzold GC, Albeanu DF, Sato TF, Murthy VN. Coupling of neural activity to blood flow in olfactory glomeruli is mediated by astrocytic pathways. Neuron. 2008; 58:897–910. [PubMed: 18579080]

Petzold GC, Murthy VN. Role of astrocytes in neurovascular coupling. Neuron. 2011; 71:782–797. [PubMed: 21903073]

Poskanzer KE, Yuste R. Astrocytic regulation of cortical UP states. Proc Natl Acad Sci U S A. 2011; 108:18453–18458. [PubMed: 22027012]

Reeves AM, Shigetomi E, Khakh BS. Bulk loading of calcium indicator dyes to study astrocyte physiology: key limitations and improvements using morphological maps. J Neurosci. 2011; 31:9353–9358. [PubMed: 21697385]

Reznichenko L, Cheng Q, Nizar K, Gratiy SL, Saisan PA, Rockenstein EM, Tanya Gonzalez T, Patrick C, Spencer B, Desplats P, Dale AM, Devor A, Masliah E. In Vivo Alterations in Calcium Buffering Capacity in Transgenic Mouse Model of Synucleinopathy. J Neurosci. 2012; 32:9992–9998. [PubMed: 22815513]

Rouach N, Koulakoff A, Abudara V, Willecke K, Giaume C. Astroglial metabolic networks sustain hippocampal synaptic transmission. Science. 2008; 322:1551–1555. [PubMed: 19056987]

Schulz K, Sydekum E, Krueppel R, Engelbrecht CJ, Schlegel F, Schroter A, Rudin M, Helmchen F. Simultaneous BOLD fMRI and fiber-optic calcium recording in rat neocortex. Nat Methods. 2012; 9:597–602. [PubMed: 22561989]

Schummers J, Yu H, Sur M. Tuned responses of astrocytes and their influence on hemodynamic signals in the visual cortex. Science. 2008; 320:1638–1643. [PubMed: 18566287]

Shen Z, Lu Z, Chhatbar PY, O'Herron P, Kara P. An artery-specific fluorescent dye for studying neurovascular coupling. Nat Methods. 2012; 9:273–276. [PubMed: 22266543]

Shi Y, Liu X, Gebremedhin D, Falck JR, Harder DR, Koehler RC. Interaction of mechanisms involving epoxyeicosatrienoic acids, adenosine receptors, and metabotropic glutamate receptors in neurovascular coupling in rat whisker barrel cortex. J Cereb Blood Flow Metab. 2008; 28:111–125. [PubMed: 17519974]

Shigetomi E, Kracun S, Khakh BS. Monitoring astrocyte calcium microdomains with improved membrane targeted GCaMP reporters. Neuron Glia Biol. 2010a:1–9. [PubMed: 20604976]

Shigetomi E, Kracun S, Sofroniew MV, Khakh BS. A genetically targeted optical sensor to monitor calcium signals in astrocyte processes. Nat Neurosci. 2010b; 13:759–766. [PubMed: 20495558]

Shigetomi E, Tong X, Kwan KY, Corey DP, Khakh BS. TRPA1 channels regulate astrocyte resting calcium and inhibitory synapse efficacy through GAT-3. Nat Neurosci. 2011; 15:70–80. [PubMed: 22158513]

Shin HK, Jones PB, Garcia-Alloza M, Borrelli L, Greenberg SM, Bacskai BJ, Frosch MP, Hyman BT, Moskowitz MA, Ayata C. Age-dependent cerebrovascular dysfunction in a transgenic mouse model of cerebral amyloid angiopathy. Brain : a journal of neurology. 2007; 130:2310–2319. [PubMed: 17638859]

Simard M, Arcuino G, Takano T, Liu QS, Nedergaard M. Signaling at the gliovascular interface. J Neurosci. 2003; 23:9254–9262. [PubMed: 14534260]

Steriade M. Grouping of brain rhythms in corticothalamic systems. Neuroscience. 2006; 137:1087–1106. [PubMed: 16343791]

Stosiek C, Garaschuk O, Holthoff K, Konnerth A. In vivo two-photon calcium imaging of neuronal networks. Proc Natl Acad Sci U S A. 2003; 100:7319–7324. [PubMed: 12777621]

Sun W, McConnell E, Pare JF, Xu Q, Chen M, Peng W, Lovatt D, Han X, Smith Y, Nedergaard M. Glutamate-dependent neuroglial calcium signaling differs between young and adult brain. Science. 2013; 339:197–200. [PubMed: 23307741]

Takano T, Tian GF, Peng W, Lou N, Libionka W, Han X, Nedergaard M. Astrocyte-mediated control of cerebral blood flow. Nat Neurosci. 2006; 9:260–267. [PubMed: 16388306]

Takata N, Mishima T, Hisatsune C, Nagai T, Ebisui E, Mikoshiba K, Hirase H. Astrocyte calcium signaling transforms cholinergic modulation to cortical plasticity in vivo. J Neurosci. 2011; 31:18155–18165. [PubMed: 22159127]

Thrane AS, Thrane VR, Zeppenfeld D, Lou N, Xu Q, Nagelhus EA, Nedergaard M. General anesthesia selectively disrupts astrocyte calcium signaling in the awake mouse cortex. Proc Natl Acad Sci U S A. 2012; 109:18974–18979. [PubMed: 23112168]

Tian P, Teng IC, May LD, Kurz R, Lu K, Scadeng M, Hillman EM, De Crespigny AJ, D'Arceuil HE, Mandeville JB, Marota JJ, Rosen BR, Liu TT, Boas DA, Buxton RB, Dale AM, Devor A. Cortical depth-specific microvascular dilation underlies laminar differences in blood oxygenation level-dependent functional MRI signal. Proc Natl Acad Sci U S A. 2010; 107:15246–15251. [PubMed: 20696904]

Turner DA, Foster KA, Galeffi F, Somjen GG. Differences in O2 availability resolve the apparent discrepancies in metabolic intrinsic optical signals in vivo and in vitro. Trends Neurosci. 2007; 30:390–398. [PubMed: 17590447]

Volterra A, Meldolesi J. Astrocytes, from brain glue to communication elements: the revolution continues. Nat Rev Neurosci. 2005; 6:626–640. [PubMed: 16025096]

Wang F, Smith NA, Xu Q, Fujita T, Baba A, Matsuda T, Takano T, Bekar L, Nedergaard M. Astrocytes modulate neural network activity by Ca(2)(+)-dependent uptake of extracellular K(+). Science signaling. 2012; 5:ra26. [PubMed: 22472648]

Wang X, Lou N, Xu Q, Tian GF, Peng WG, Han X, Kang J, Takano T, Nedergaard M. Astrocytic Ca(2+) signaling evoked by sensory stimulation in vivo. Nat Neurosci. 2006; 9:816–823. [PubMed: 16699507]

Wang, X.; Takano, H.; Nedergaard, M. Astrocytic calcium signaling: mechanism and implications for functional brain imaging. In: Hyder, F., editor. Dynamic brain imaging: multi-modal methods and in vivo applications. Vol. 489. Humana Press; 2009.

Winship IR, Plaa N, Murphy TH. Rapid astrocyte calcium signals correlate with neuronal activity and onset of the hemodynamic response in vivo. J Neurosci. 2007; 27:6268–6272. [PubMed: 17554000]

Zonta M, Angulo MC, Gobbo S, Rosengarten B, Hossmann KA, Pozzan T, Carmignoto G. Neuron-to-astrocyte signaling is central to the dynamic control of brain microcirculation. Nat Neurosci. 2003; 6:43–50. [PubMed: 12469126]

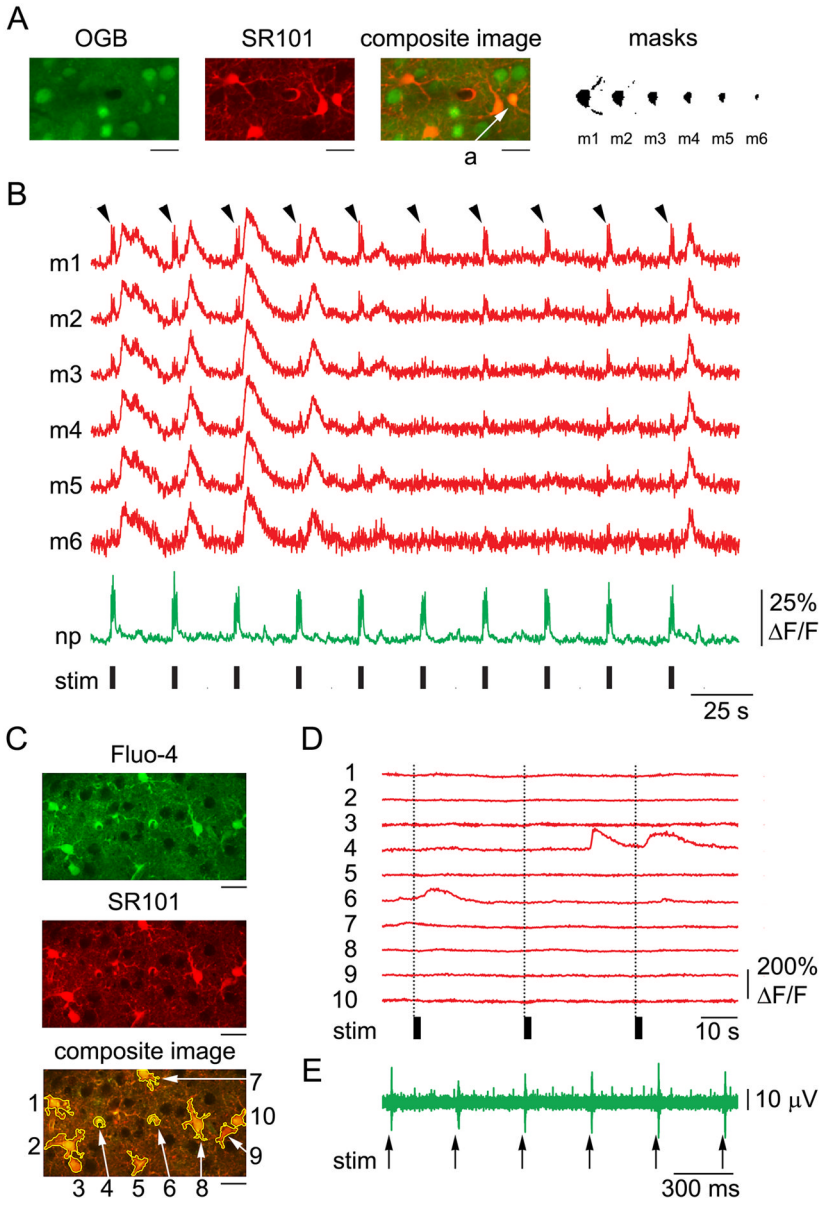

Fig. 1. Cross-talk between astrocytic and neuropil calcium signals during stimulus-induced response

A, Reduction of cross-talk with neuropil signals through shrinking ("erosion") of astrocytic ROI in OGB1-stained cortex. An example FOV including a number of astrocytes labeled with SR101/OGB1 and a number of neuronal cell bodies labeled with OGB1, imaged 190 μm below the cortical surface. The scale bar is 20 μm. A gradual erosion of a single-cell ROI (astrocytic cell body labeled "a") is illustrated on the right: Starting from a mask defined by a liberal thresholding of SR101 intensity (m1) and eroding a single layer of pixels at a time (m2-6). The masks are enlarged relative to the composite image for viewing purposes.

B, Time-courses extracted from the masks shown in (A). All time-courses are baseline-subtracted and peak-normalized to illustrate that the erosion procedure selectively decreases contamination from neuropil (black arrowheads) while preserving the slow and large-amplitude "true" astrocytic signal. Calcium signal change in neuropil (i.e., outside neuronal

and astrocytic cell bodies), expressed as ΔF/F, is shown in green. The black bars indicate stimulus duration.

C, An example FOV labeled with Fluo-4 and SR101, imaged 180 μm below the cortical surface. The yellow color of the composite image indicates co-localization of Fluo-4 (green) and SR101 (red) in astrocytes. The scale bars are 30 μm.***D,*** Calcium signal time-courses, expressed as ΔF/F, extracted from the ROIs outlined in the composite image in (C). The black bars indicate stimulus duration.

E, An example nonrectified MUA voltage trace illustrating responses to six consecutive stimuli within a single stimulus trial. MUA recordings were performed simultaneously with optical acquisition to ensure neuronal response to stimulation.

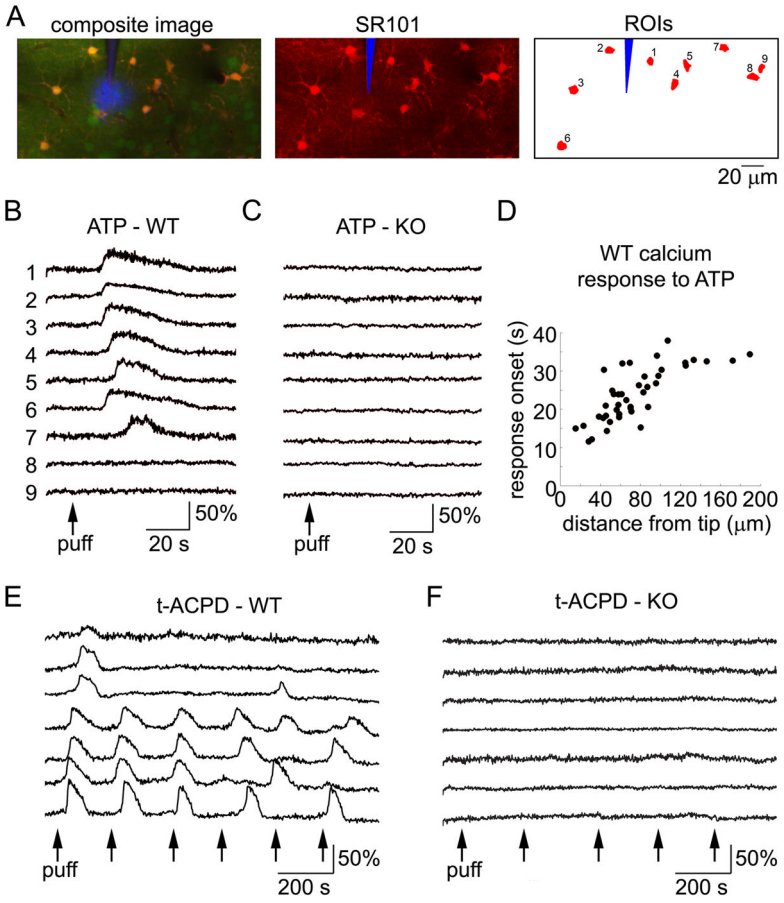

Fig. 2. IP_3R2-KO mice do not exhibit IP3-mediated calcium increases

A, Example response to microinjection of 1-mM ATP imaged 100 μm below the cortical surface in a WT subject. Left: A composite image of OGB1 (green), SR101 (red), and the injection micropipette (blue). Right: Astrocytic ROIs. The scale bar is 20 μm.

B, Calcium signal time-courses extracted from astrocytic ROIs in (A).

C, As in (B) for an IP_3R2-KO subject. Every line represents a time-course from an individual astrocytic cell body. Composite image and ROIs are not shown.

D, Onsets of astrocytic calcium increases in response to ATP in WT subjects, as a function of distance from the injecting pipette. Astrocytes in IP_3R2-KO subjects did not exhibit calcium increases and are not plotted.

E, Example response to microinjection of 10-μM t-ACPD imaged 120 μm below the cortical surface in a WT subject: The first 3 puffs evoked time-locked calcium increases followed by irregular oscillations.

F, As in (E) for an IP_3R2-KO subject.

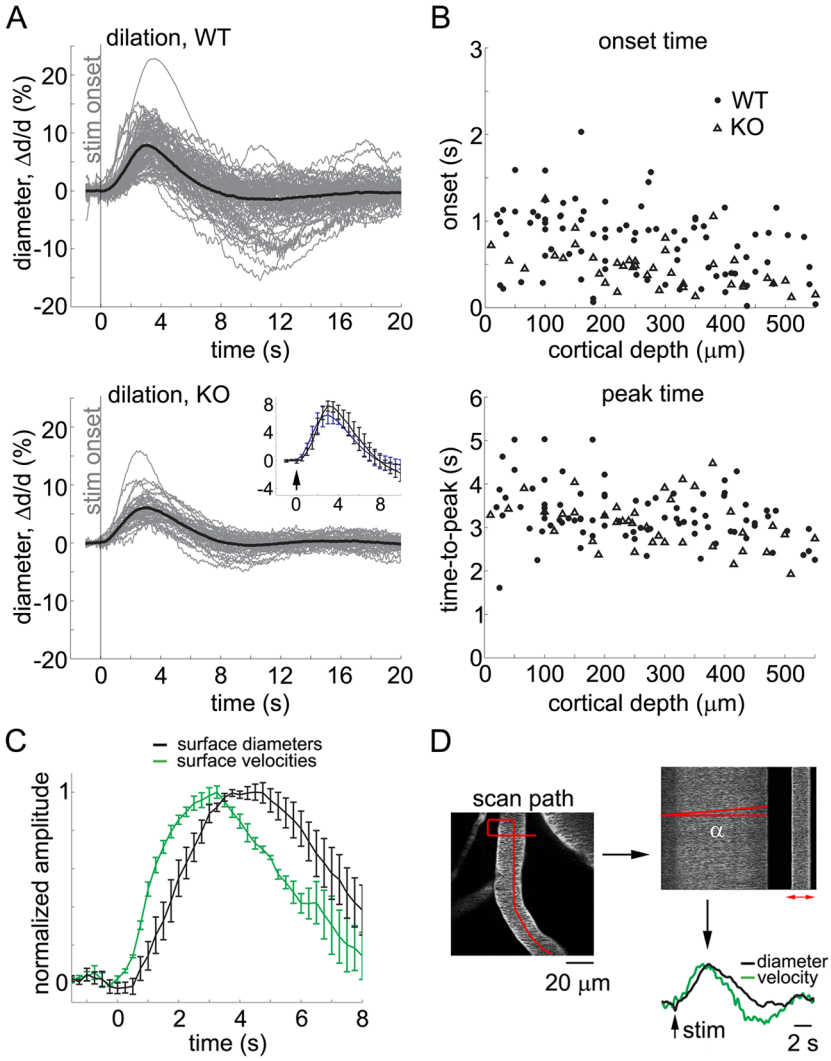

Fig. 3. IP_3R2-KO mice exhibit normal functional hyperemia

A, Time-courses of arteriolar diameter change in WT and IP_3R2-KO subjects (top and bottom panels, respectively). All measurements for each category are overlaid. The average is superimposed on each panel (thick lines). The stimulus onset is indicated by the gray vertical line. The across-subject averages are superimposed in the inset to facilitate temporal comparison; the error bars indicate a 95% confidence interval for the mean.

B, Onset (top) and time-to-peak (bottom) for all measured arteriolar diameter changes in WT (solid dots) and IP_3R2-KO (open triangles) subjects, extracted from the data in (A). Data from all subjects are overlaid and presented as a function of the cortical depth.

C, Comparison of paired diameter and velocity measurements from surface arterioles. Cross-subject averages for diameter (black) and velocity (green) time-courses. First, we averaged all time-courses acquired within a subject. Then, averaged time-courses were normalized by the peak amplitude before calculating the average across subjects; the error bars indicate standard error across subjects. An increase in velocity preceded an increase in diameter ($p<0.01$). This behavior is consistent with a theoretical expectation from a distributed vascular network when the fastest dilation occurs in deep cortical layers (Boas et al., 2008).

D, An example illustrating simultaneous measurements of diameter and velocity. On the left, a scan path is superimposed in red on an FITC image of a surface arteriole. A segment of the

scan path along the vessel is used to estimate velocity based on the angle of streaks in temporally stacked lines denoted by α at the top right (see **Materials and Methods**) (Kleinfeld et al., 1998). A segment of the scan path across the vessel is used to compute dilation based on expansion of the profile (the red arrow at the top right). Corresponding diameter (black) and velocity (green) time-courses are shown at the bottom right.

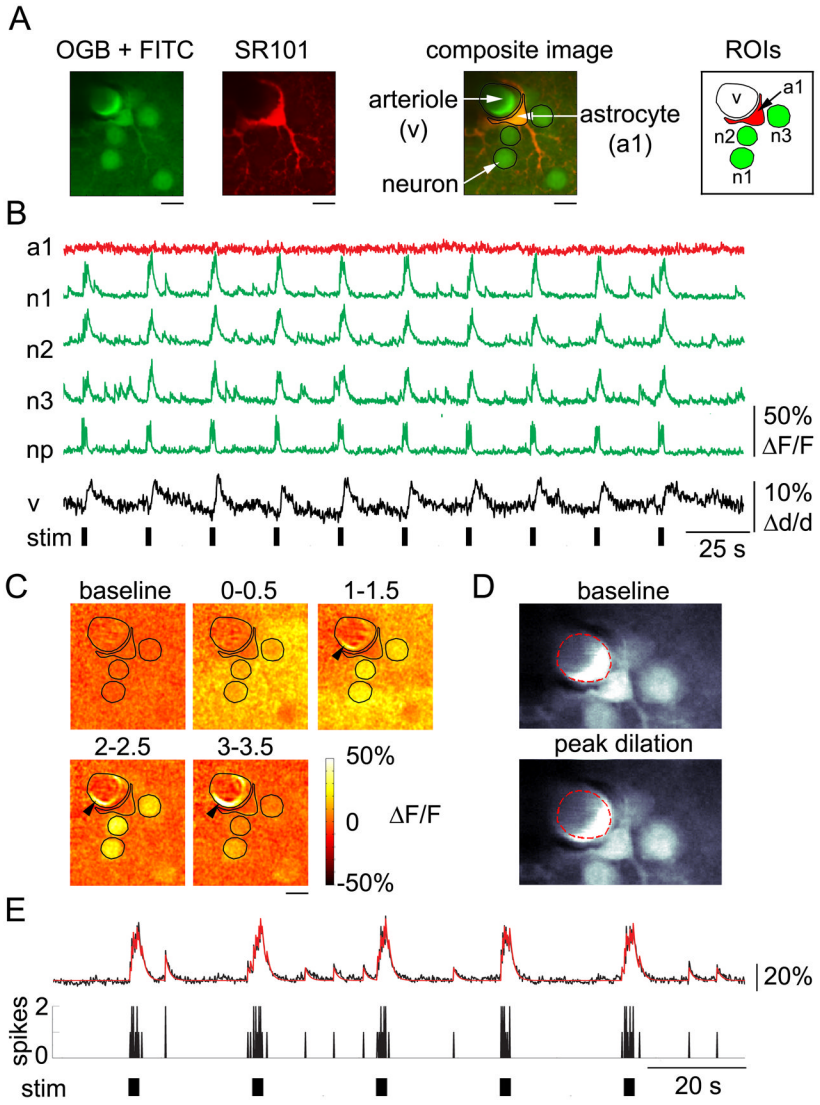

Fig. 4. Robust arteriolar dilation is observed in the absence of an astrocytic calcium response

A, Representative FOV including a perivascular astrocyte labeled with SR101/OGB1, a diving arteriole labeled by intravascular injection of FITC, and a number of neuronal cell bodies labeled with OGB1, imaged 150 μm below the cortical surface. ROIs used for extraction of time-courses are shown on the right.

B, Time-courses extracted from the ROIs shown in (A). Astrocytic (red) and neuronal (green) calcium signal changes are expressed as ΔF/F. Vasodilation is expressed as percent diameter change relative to the baseline diameter, Δd/d. The diameter change was extracted from the expansion of FITC-labeled intravascular lumen, indicated by "v" in (A). The black bars indicate stimulus duration.

C, Ratio images showing neuronal signal change and vasodilation (black arrowheads) in response to the first stimulus trial. The ROI contours are overlaid. Each image was computed as an average of 5 consecutive ratio frames. The corresponding time windows relative to the stimulus onset (in seconds) are indicated above the images. Note the 0.5-s gap between the consecutive images. The scale bars in (A) and (C) are 10 μm.

D, "Raw" trial-averaged images of the upper part of the FOV illustrating the expansion of FITC-labeled cross-section during peak dilation (bottom) relative to the pre-stimulus baseline (top, the red dotted line). The green channel is shown.

E, Representative example of a calcium signal time-course extracted from a single neuronal cell body (black trace) (labeled "n1" in (B)). Calcium signal changes are expressed as $\Delta F/F$. A computational fit to the data is overlaid in red. The fitting procedure assumed a convolution kernel with τ=0.8s. The black bars at the bottom indicate stimulus duration. As a general rule, neurons fired 1–2 spikes in response to each of 6 electrical pulses in the stimulus train.

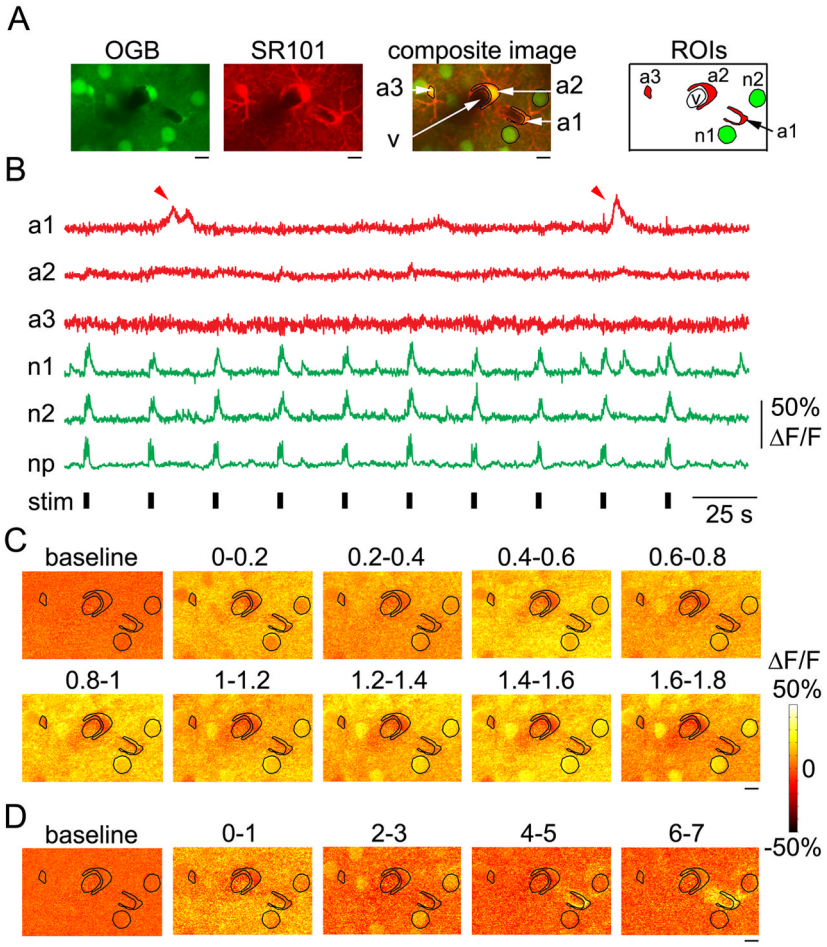

Fig. 5. Astrocytes exhibit occasional calcium responses to individual stimulus trials

A, Example FOV 20 μm below an arteriolar branching point including 3 astrocytic ROIs, imaged 200 μm below the cortical surface. No intravascular FITC was present.

B, Time-courses extracted from astrocytic and neuronal ROIs shown in (A). Red arrowheads point to a calcium increase in one of the ROIs (a1) during 2 of 10 stimulus trials.

C, Trial-averaged ratio images for the first 1.8 s following the stimulus onset during the neuronal response. Every image is an average of 2 consecutive frames. Intensity fluctuations between consecutive images reflect temporally undersampled “flashing” of the neuropil and neuronal cell bodies in response to repetitive stimuli (6 individual stimuli at 3 Hz). The ROI contours from (A) are overlaid. The corresponding time windows relative to the stimulus onset (in seconds) are indicated above the images.

D, Ratio images for the ninth stimulus trial featuring calcium response in the astrocytic ROI labeled a1. Time relative to the stimulus onset (in seconds) is indicated above the images. Note the 1-s gap between the consecutive images. The scale bars in (A), (C) and (D) are 10 μm.

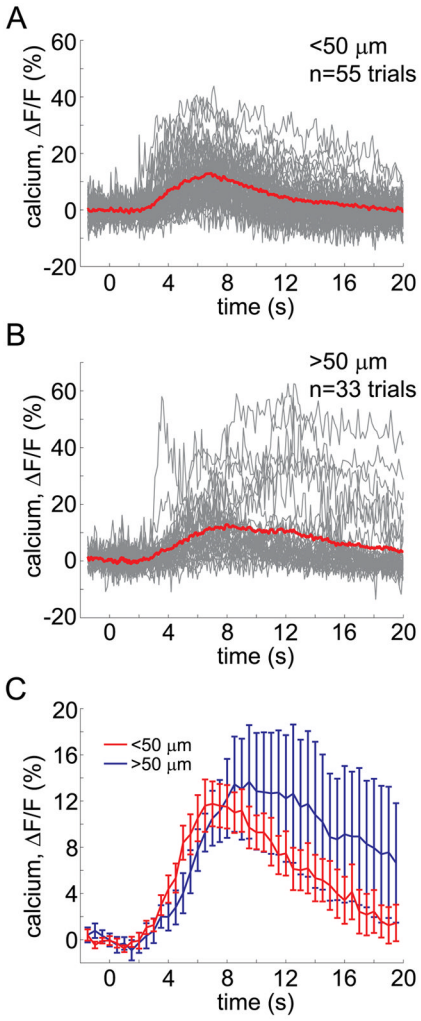

Fig. 6. Astrocytic response kinetics as a function of the distance from arterioles

A–B, Overlaid time-courses of all trials with significant astrocytic signal change, pooled across subjects, sorted by distance from diving arterioles: within (A) and outside (B) a 50-μm radius.

C, Statistical comparison of astrocytic response kinetics for the 2 distance categories across subjects: <50 μm (red) and >50 μm (blue). The curves show across-subject averages; the error bars indicate standard error.

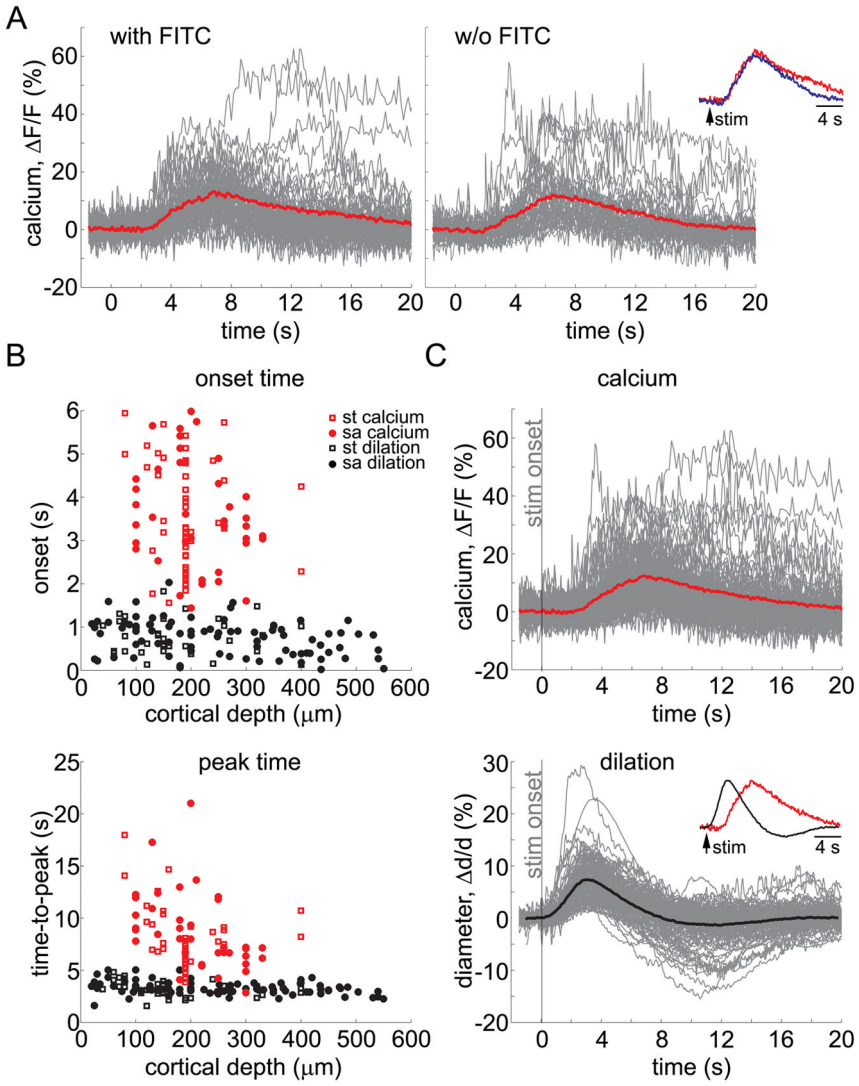

Fig. 7. Astrocytic calcium increase is delayed relative to arteriolar dilation

A, Overlaid time-courses of all trials with significant astrocytic signal change, pooled across subjects with (left) and without (right) intravascular FITC used for simultaneous measurements of vasodilation.

B, Onset (top) and time-to-peak (bottom) for all measured astrocytic calcium responses (red) and arteriolar diameter changes (black). Data from all subjects are overlaid and presented as a function of cortical depth. Open squares and solid dots correspond to simultaneous (st) and stand-alone (sa) measurements, respectively. Simultaneously measured diameters are included regardless of the presence of an astrocytic calcium response.

C, Time-courses of astrocytic calcium change (top) and arteriolar diameter change (bottom). An average is superimposed on each panel (thick lines). The stimulus onset is indicated by the gray vertical line. Peak-normalized averages are superimposed in the inset to facilitate temporal comparison.

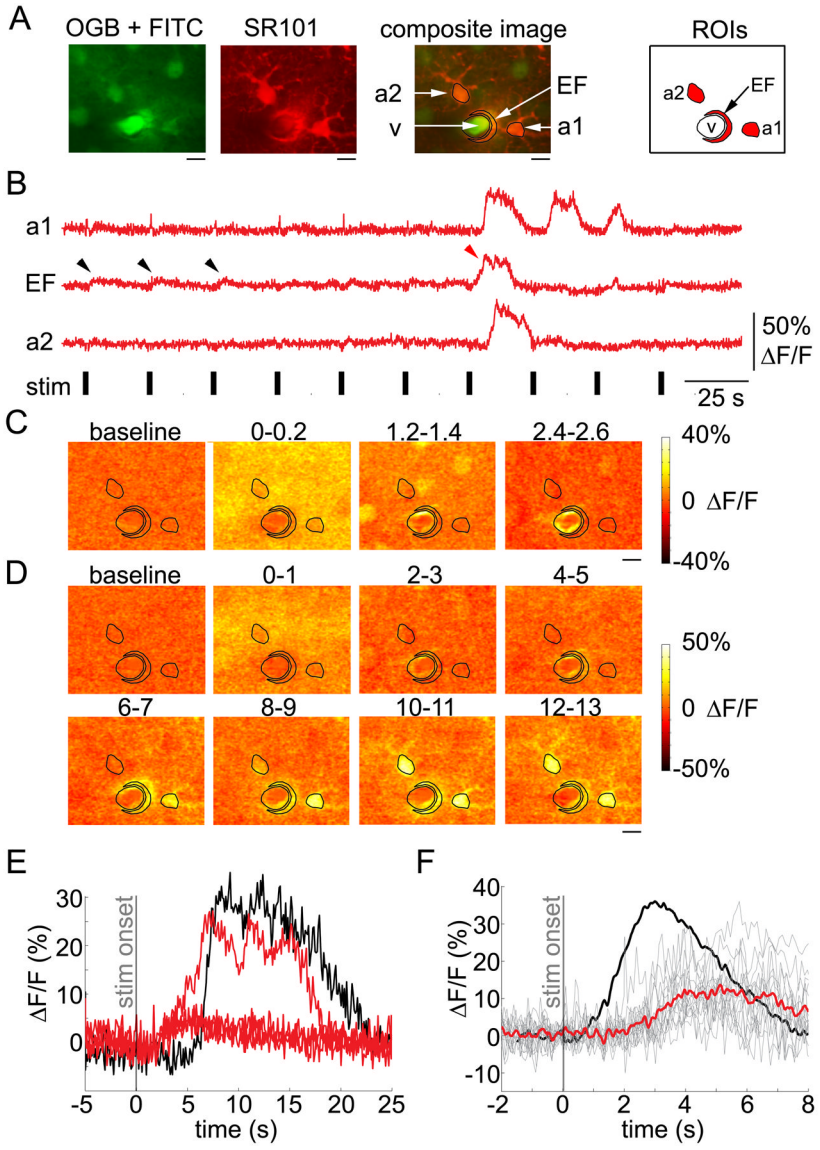

Fig. 8. Calcium increase in astrocytic endfeet lags behind dilation onset

A, An example FOV including 2 astrocytes, one (a1) with a connected endfoot (EF), imaged 260 μm below the cortical surface.

B, Time-courses extracted from ROIs shown in (A). The red arrowhead points to a calcium increase in the endfoot in response to the seventh stimulus trial.

C, Trial-averaged ratio images for the first ~2.5 s following the stimulus onset during the neuronal response. Every image is an average of 2 consecutive frames. The ROI contours from (A) are overlaid. The corresponding time windows relative to the stimulus onset (in seconds) are indicated above the images. Note the 1-s gap between the consecutive images.

D, Ratio images in response to the seventh stimulus trial. The ROI contours are overlaid. Each image was computed as an average of 10 consecutive ratio frames. The corresponding time windows relative to the stimulus onset are indicated above the images. Note the 1-s gap between the consecutive images. The scale bars in (A), (C) and (D) are 10 μm.

E, Overlaid time-courses of astrocytic calcium change in the cell body (a1, black) and the connected endfoot (EF, red).

F, All responsive endfoot trials are overlaid. The average is shown in thick red. The averaged dilation time-course from the same depth category (180–300 μm), normalized to the maximum amplitude of the calcium traces, is superimposed in thick black.

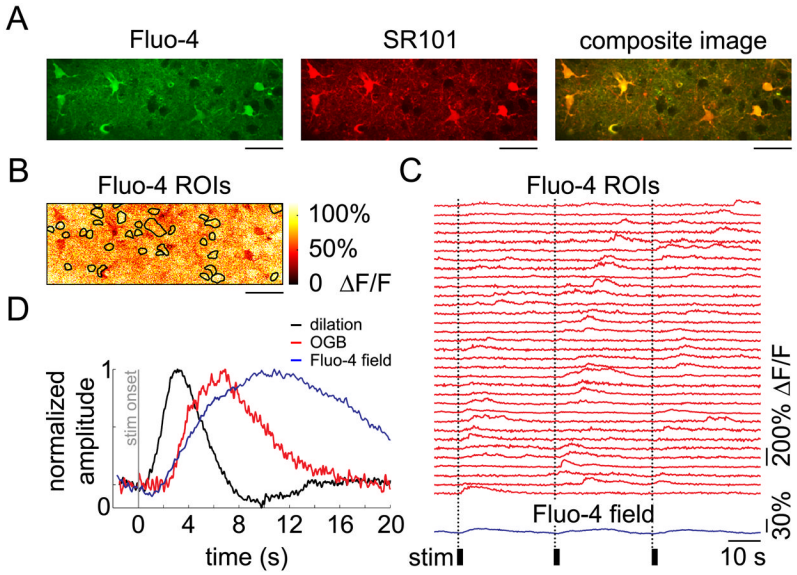

Fig. 9. Calcium increase in fine astrocytic arborizations lags behind dilation onset

A, An example FOV labeled with Fluo-4 and SR101, imaged 200 μm below the cortical surface.

B, Sub-cellular ROIs overlaid on an MIP image of Fluo-4 ratio images. The MIP image was calculated for the time series of 3 stimulus trials. Individual ROIs were defined by thresholding MIP images calculated for individual stimulus trials. The scale bars in (A) and (B) are 50 μm.

C, Calcium signal time-courses extracted from ROIs shown in (B) (red traces) and from the entire FOV ("Fluo-4 field," blue trace). The black bars indicate stimulus duration.

D, Averaged Fluo-4 field response. Averaged dilation time-course and calcium response from astrocytic cell body ROIs from the same depth category (≤200 μm) are superimposed in black and red, respectively. All curves are normalized to the maximum amplitude.